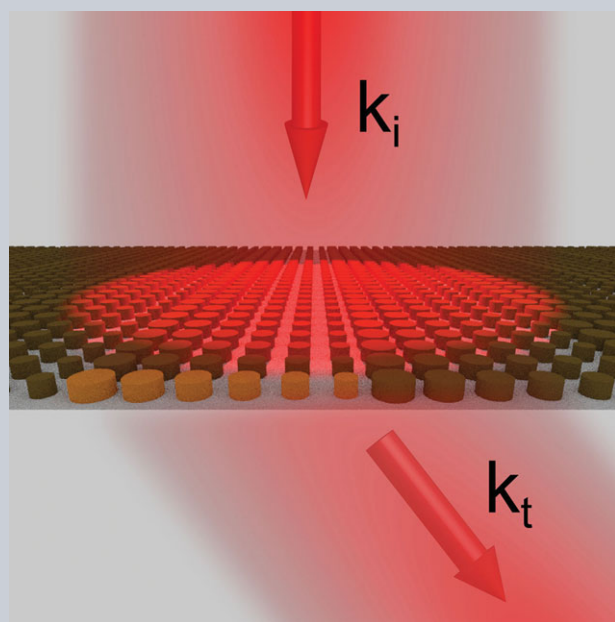


Abstract Recently, metasurfaces have received increasing attention due to their ability to locally manipulate the amplitude, phase and polarization of light with high spatial resolution. Transmissive metasurfaces based on high-index dielectric materials are particularly interesting due to the low intrinsic losses and compatibility with standard industrial processes. Here, it is demonstrated numerically and experimentally that a uniform array of silicon nanodisks can exhibit close-to-unity transmission at resonance in the visible spectrum. A single-layer gradient metasurface utilizing this concept is shown to achieve around 45% transmission into the desired order. These values represent an improvement over existing state-of-the-art, and are the result of simultaneous excitation and mutual interference of magnetic and electric-dipole resonances in the nanodisks, which enables directional forward scattering with a broad bandwidth. Due to CMOS compatibility and the relative ease of fabrication, this approach is promising for creation of novel flat optical devices.



High-transmission dielectric metasurface with 2π phase control at visible wavelengths

Ye Feng Yu^{*,**}, Alexander Y. Zhu^{**,*}, Ramón Paniagua-Domínguez, Yuan Hsing Fu, Boris Luk'yanchuk, and Arseniy I. Kuznetsov^{*}

1. Introduction

Recent years have witnessed significant research work in the area of optical metamaterials, broadly defined as artificially synthesized media engineered at a size scale much smaller than the wavelength of incident light. In contrast to conventional materials whose intrinsic properties are fixed, metamaterials open up the exciting possibility of tailoring material properties to a specific application. Consequently numerous functionalities and devices have been developed, such as negative refractive index lenses, optical cloaking devices, artificial magnets, nanolasers, spasers and more [1].

Metasurfaces [2], which can be understood as a two-dimensional version of metamaterials, have garnered particular attention due to their advantages of possessing a smaller physical footprint, simpler fabrication and lower losses compared to their bulk counterparts. Crucially, they retain the ability to manipulate the phase, amplitude and polarization of light upon transmission or reflection. Due to their two-dimensional nature, it is therefore possible to

realize planar analogs of traditional optical components, such as lenses, beam transformers, broadband pass filters, wave plates and polarization converters [2–4]. In addition, new functionalities arising from phase discontinuities at an interface can also be obtained, such as beam deflection [5–7], beam forming [8–12], and holography [13–15].

Plasmonic-based metasurfaces achieve the required full 2π phase control primarily using two different approaches. The first approach relies on the generation of two resonances, which can be independently tuned, each covering a standard phase range of π . For example, V-shaped antennas with different arm lengths and angles can generate symmetric and asymmetric modes. Full wavefront control can be achieved by varying the geometry of the antennas, which also takes into account material dispersion effects [6, 12]. The second approach is based on rotationally asymmetric nanostructures whose resonant modes are polarization dependent. Complete phase control can be achieved by spatially varying the geometric orientation of the nanostructures, due to phase singularity via the Pancharatnam–Berry phase [16]. However, the

Data Storage Institute, A*STAR (Agency for Science, Technology and Research), 5 Engineering Drive 1, 117608, Singapore

^{**}Equal contribution

^{*}Corresponding authors: e-mails: yu_yefeng@dsi.a-star.edu.sg, arseniy_k@dsi.a-star.edu.sg

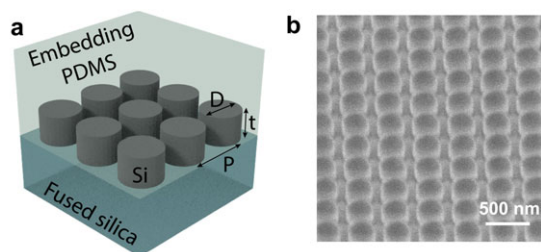


Figure 1 (a) Schematic of the dielectric metasurface consisting of an array of silicon nanodisks on top of a fused silica substrate and embedded into a PDMS layer from the top to realize refractive index matching. (b) Example of the fabricated nanodisk array: tilted view (52°) SEM image, showing good uniformity, edge profile and approximately 90-nm interparticle gaps.

intrinsically high losses of metals at optical frequencies lead to low performance efficiencies for plasmonic metasurfaces, especially in transmission [17, 18]. This initiated significant work in developing dielectric analogs of metasurfaces, since many dielectric materials have very low absorption loss in the visible and near-infrared range. If the refractive index of a dielectric material is sufficiently high (e.g. >2) in the spectral range of interest, nanoparticles made of this material may possess strong Mie-type scattering resonances analogous to their plasmonic counterparts [19, 20]. Accordingly, various high-index dielectric structures have been proposed and in some cases demonstrated at optical frequencies, but have yet to unequivocally show transmission coefficients and bandwidths significantly superior to their metallic counterparts [8–10, 21–27].

In this work, we provide clear theoretical and experimental proof that close-to-unity resonant transmission can be achieved at visible wavelengths using properly designed high-index (amorphous silicon) metasurfaces (Fig. 1). This effect is realized by almost complete suppression of resonant reflection due to destructive interference between electric and magnetic-dipole resonances. These transparent metasurfaces have resonant behavior and allow for precise engineering in 2D of the local transmitted light phase over the whole 2π range. The latter concept is demonstrated by the example of a gradient metasurface having close to 50% transmission into the desired diffraction order. The maximum transmission is limited by material loss and can further be improved, e.g. by using other materials with lower losses in the visible (e.g. TiO_2 , GaN, etc.).

It is known [19, 20, 28–32] that in spherical high refractive index dielectric particles, a strong magnetic dipole response is observed in addition to the electric one. This resonance appears when the wavelength of light in a particle is close to the diameter $\lambda/n_{\text{mat}} \approx D$ [30]. This corresponds to the condition where the polarization of the incident electric field is antiparallel at opposite boundaries of the sphere, which gives rise to strong coupling of light to circulating displacement currents within the particle, resulting in generation of a strong magnetic dipole in the center. Dielectric nanoparticles with a magnetic dipole response can be used as building blocks for metamaterials with nonunity

magnetic permeability [19, 28, 29]. Additionally, it was theoretically predicted [33] and experimentally demonstrated [34, 35] that at particular wavelengths such particles may possess strong directional forward scattering with almost zero backscattering. This effect appears when the electric and magnetic-dipole resonances have similar amplitudes and phases, interfering constructively in the forward direction while canceling each other in the backscattering direction. This is known as the first Kerker's condition, and was theoretically proposed for spherical particles having nonzero magnetic susceptibility in 1983 [36]. In addition, recent work on oblate dielectric spheroids [37] and disks [23] has shown that these geometries have significantly greater overlap of electric and magnetic-dipole resonances, resulting in the realization of Kerker's condition across a relatively broad spectral bandwidth. A metasurface composed of such densely packed nanoparticles with zero resonant backscattering may thus have almost zero reflection and transmission close-to-unity over the dipole resonance spectral range, while having a controllable phase shift in transmission over $0-2\pi$ due to excitation of two (electric and magnetic) dipoles.

The idea of transparent dielectric metasurfaces with 2π phase control was recently proposed in [23, 24] and an attempt has been made to realize this effect in the near-IR spectral range with silicon on insulator (SOI)-based nanostructures. However, the maximum experimentally achieved broadband resonant transmission was around 55%. Here, we experimentally demonstrate that close to 90% transmission can be achieved with silicon-on-quartz metasurfaces even in the visible spectrum while maintaining 2π phase control. We also verify this by observing highly efficient (close to 50%) beam deflection with such metasurfaces, which is experimentally demonstrated.

2. Near-unity visible transmission of uniform silicon nanodisk arrays

Our metasurface (Fig. 1) consists of an array of silicon nanodisks of 130 nm thickness (t) and variable diameters ($D = 2R$) with subwavelength period ($P = D + 90$ nm) on a fused silica substrate. The structure is embedded in a poly-dimethyl-siloxane (PDMS) layer from the top. For a certain particle diameter range this configuration fulfills the condition for minimized reflection, which happens when the spectral positions of electric and magnetic-dipole resonances are matched. For materials with a refractive index close to 3.7, this occurs at a ratio of diameter to height of approximately 2 [23, 34, 37]. PDMS was used as an embedding medium to simulate conditions close to a homogeneous environment that enables better amplitude matching between the two resonant modes. The height of 130 nm was chosen to have the resonances in the red spectral range of 700–800 nm where intrinsic absorption loss of our amorphous silicon is small. The exact values for these parameters were obtained via finite-difference time-domain (FDTD, Lumerical) simulations and optimization sweeps,

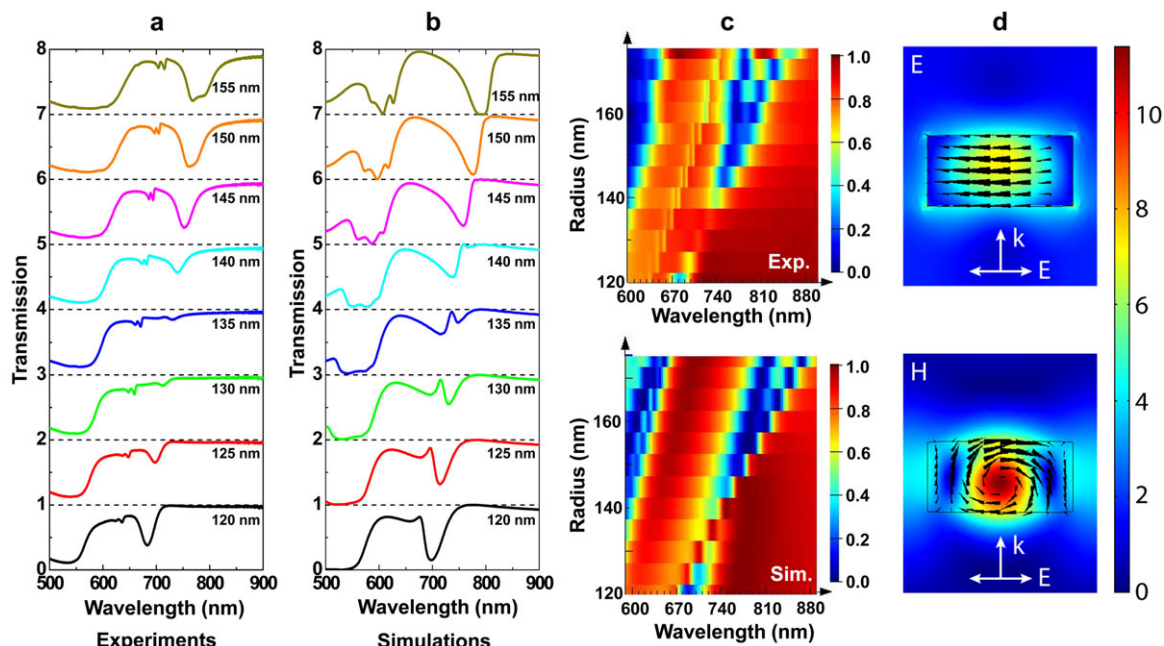


Figure 2 (a) Experimentally measured and (b) simulated transmission spectra of silicon nanodisk arrays with varied disk radius (R) and array period $P = 2R + 90$ nm (respective radii values are shown in the insets). Curves for each size are plotted with a vertical offset of unity. It is observed that the experimental and theoretical data are in good agreement. (c) The same experimental (top) and simulated (bottom) data for a larger disk radii range shown in contour plots to illustrate the tuning of the respective spectral positions of electric- and magnetic-dipole resonances. (d) Near-field maps of a cross section of the optimized disk array (disk radius = 135 nm, array period = 360 nm) at the wavelength of transmission maximum of 736 nm, showing electric (top) and magnetic (bottom) field amplitudes normalized to the incoming plane wave values. The magnitude and direction of displacement currents are shown by the black arrows in both images.

using experimentally measured refractive-index data of our silicon deposited by chemical vapor deposition (CVD) (see Methods in Supplementary Information).

Experimentally measured and simulated transmission spectra of the arrays of silicon disks used for the optimization sweeps (with radii varying from 120 nm to 155 nm) are presented in Fig. 2. For smaller sizes of nanodisks (e.g. radius below 130 nm) as shown in Figs. 2a and c (top), it is seen that the electric and magnetic dipoles are spectrally close but not fully overlapped and give a resonant dip in transmission around 680–700 nm. However, as the disk size is increased, the dipole resonances overlap and the transmission at resonance increases. The optimal transmission case is reached for radii of 130–135 nm with peak transmission close to 90% around 700 nm and > 85% transmission across the whole resonant range from 670 nm to 770 nm. With larger disk sizes, the resonances are again detuned, resulting in a characteristic crossing of the resonances [23, 24, 37] and decreased resonant transmission. Figures 2b and c (bottom) show numerically calculated results via FDTD for similar disk sizes. It is seen that the simulated and experimental spectra are in a good agreement, in terms of both feature intensity and position. Magnified views of experimental transmission spectra for different disk radii varied in the range from 120 nm to 175 nm with a step of 5 nm are shown in supplementary materials (Fig. S1). Though the transmission through the arrays

at optimized conditions ($R = 135$ nm) is close-to-unity all nanoparticles are resonantly excited having both spectrally overlapped electric and magnetic-dipole resonances (see Fig. 2d showing resonant electric and magnetic near-fields at the wavelength of transmission maximum of 736 nm).

Figure 3a shows in greater detail the experimentally measured transmission for the optimal parameters of the silicon nanoparticle array (corresponding to $R = 135$ nm in Fig. 2a), while Fig. 3b plots the optimal simulated response (bottom panel) as well as the corresponding electric- and magnetic-dipole contributions (top panel) extracted through the multipole decomposition technique [38, 39] (see Methods in Supplementary Information). One can see a reasonable agreement between the experiment and simulations. Indeed, we observe a peak in transmission close to 90% on resonance, in good agreement with simulated values. However, the experimental transmission over the whole resonant range from 670 nm to 770 nm is surprisingly higher than that in the simulations. This is likely due to the narrower and stronger electric-dipole contribution, which does not fully overlap with the broader magnetic-dipole resonance in the simulated case. In the experiment the electric-dipole resonance broadens due to fabrication tolerances, including surface roughness, size variations and slight sidewall tapering (which could be aperiodic), as well as deviations from bulk-material parameters. All these factors may affect the Q-factor and intensity of the electric-dipole resonance

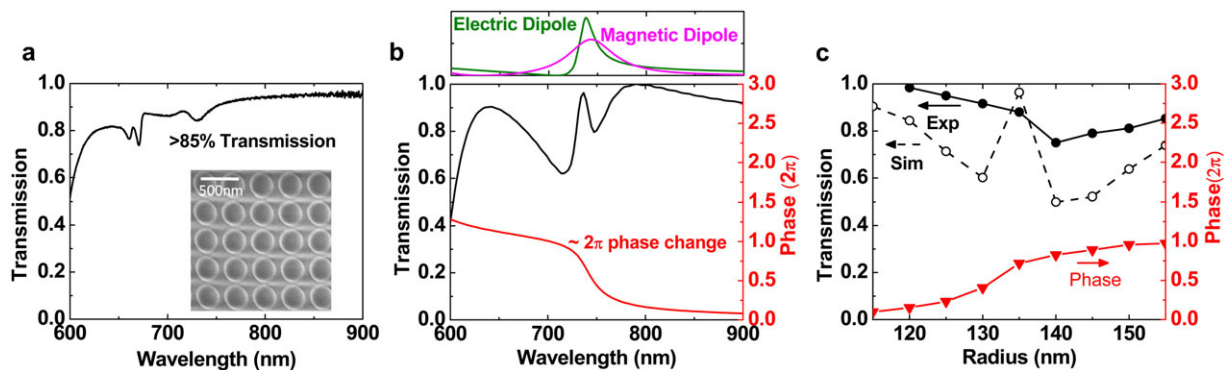


Figure 3 (a) Experimentally measured spectrum of the fabricated silicon nanodisk array with disk radius of 135 nm and optimal transmission (see also Fig. 2a). (Inset) Top view SEM image of the array. (b) (Bottom panel) Numerically simulated transmission curve (black line) for the silicon array with optimized parameters: disk height of 130 nm, radius of 135 nm, array pitch of 360 nm, shown together with the corresponding phase change (red line) which covers a full period from 0 to 2π due to the spectral overlap of the two resonances. The phase response is normalized by subtracting that of a “blank” sample, i.e. substrate and embedding medium without the nanodisk arrays. (top panel) Electric- and magnetic-dipole contributions obtained via multipole decomposition of modes excited inside each single particle in the array. Relative amplitudes of the electric and magnetic resonances are preserved. (c) Numerically calculated (dashed black line with open circles) and experimentally measured (solid black line with filled circles) transmission at optimized wavelengths of 736 nm and 720 nm, respectively. The optimized wavelengths in simulations and experiment were chosen at the highest transmission value at the resonance for the particle radius of 135 nm. The discrepancy in wavelengths arises from slightly different resonance positions in simulation and experiment. The phase shift retrieved from numerical simulations at 736 nm is also shown (solid red line with filled triangles). It is seen that as the disk size varies in a small range from 115 nm to 155 nm reasonably high transmission and full 2π phase control can be achieved. This demonstrates the extension from a uniform array to a transmissive metasurface with beam-forming capabilities. Phase response is obtained from simulations and normalized in the same way as in (b).

and result in its better matching with the magnetic dipole in the experiment. We also remark that near-field interaction between the nanoparticles in the array strongly influences the spectral positions of both electric and magnetic-dipole resonances. This also results in significant narrowing of the electric-dipole resonance in the array, while the magnetic-dipole resonance shape is less affected due to the stronger field confinement inside the particles. This is illustrated in Fig. S2 in the supplementary materials, where the same simulation is shown for the case of an isolated nanodisk. Thus, small deviations from ideal periodicity could also contribute to better overlap of the resonances.

Figure 3b also shows the simulated phase change in the silicon nanoparticle array over a full period of $0-2\pi$ around the resonance, as expected due to the overlap of the electric- and magnetic-dipole contributions. To design a metasurface with a full phase control at a particular wavelength, one approach is to vary the disk size around the optimized position. This is demonstrated in Fig. 3c both in simulations and experiment for disk radius variations around the central value of 135 nm. Transmission through the arrays with different nanoparticle size is shown at optimized wavelengths, which are slightly different in simulations and experiments, of 736 nm and 720 nm respectively, due to a minor offset in resonance position between the two. A simulated phase change at 736 nm is also shown in Fig. 3c as a function of disk radius. One observes that the phase of the transmitted light varies in the range of 2π when the disk radius is changed from 115 nm to 155 nm, while reasonably high transmission centered at the optimal value can be achieved. Note that the transmission plots as a function of

nanoparticle size exhibit a similar behavior to those plotted as a function of wavelength since small variations in size tend to linearly shift the resonance features. This causes the simulated transmission curve in Fig. 3c to exhibit double-dip behavior, similar to Fig. 3b, whereas the experimental curve has a smoother profile, similar to Fig. 3a. Overall, these results demonstrate that with a proper choice of particle sizes, the extension from a uniform array to a metasurface with beam forming capabilities and overall high transmission can be achieved.

3. Gradient metasurface and beam deflection

To validate the phase control effect of these transparent silicon nanodisk arrays, we utilized a gradient metasurface with a supercell containing 8 elements, whose radius is increased from 120 nm to 155 nm in steps of 5 nm. The period of the nanodisk array is fixed at 360 nm and the height of the nanostructures is 130 nm (Fig. 4a). These sizes were chosen to provide the accumulated phase difference of approximately $\frac{\pi}{4}$ from one neighboring element to the other, resulting in a full 2π phase difference accumulation over the period of the supercell. According to the generalized Snell's law: $\sin(\theta_t)n_t - \sin(\theta_i)n_i = \left(\frac{\lambda_0}{2\pi}\right) \times \left(\frac{d\Phi}{dx}\right)$, [6], where the θ_t/θ_i is the transmitted/incident angle, n_t/n_i is the refractive index of surrounding medium on transmitted/incident sides, λ_0 is the radiation wavelength in vacuum and $d\Phi/dx$ is the (spatial) phase gradient, we expect that for our experimental

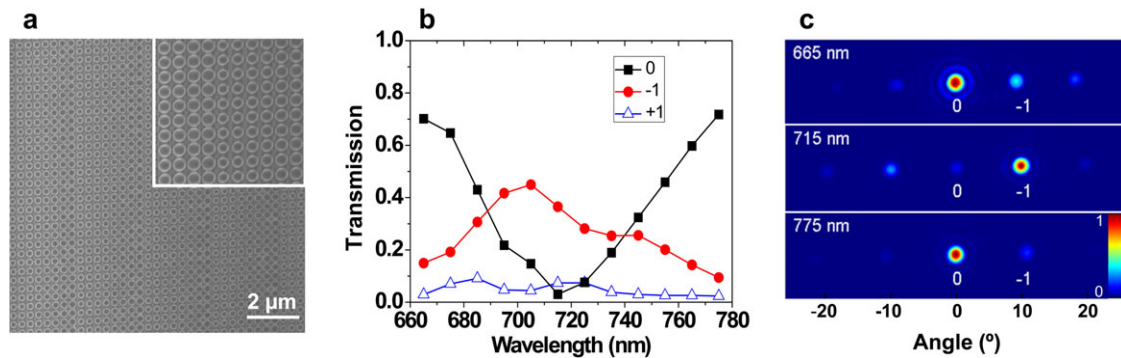


Figure 4 (a) Top-view SEM image of a gradient metasurface used for beam-deflection experiments. Each supercell consists of 8 nanodisk elements of varying radii ranging from $R = 120$ nm to 155 nm, in steps of 5 nm. The array period is kept constant at 360 nm. The inset shows the magnified view. (b) Experimentally measured amplitudes of 0^{th} , -1 and $+1$ diffraction orders (black filled squares, red filled circles and blue open triangles, respectively) normalized to the intensity of the beam transmitted through the blank substrate without the metasurface. (c) Images taken in the back focal plane of the collection objective at 665 nm, 715 nm and 775 nm (top to bottom, respectively) normalized to the maximum intensity in each image. It is seen that at a working wavelength of 715 nm most of the power is coupled into -1 order corresponding to the expected beam-deflection behavior.

configuration (see Methods in Supplementary Information), the metasurface will deflect the transmitted beam at an angle of 10.3° in resonance.

Experimental measurements of the beam deflection conducted through back-focal plane imaging of light transmitted through the metasurface are shown in Figs. 4b and c (see Methods in Supplementary Information for experimental details). We scan the wavelength of incident beam over the collective (electric and magnetic) resonance position in steps of 10 nm. At shorter wavelengths (see 665 nm in Fig. 4c), a regular diffraction pattern is observed in transmission with significant energy accumulated in the 0^{th} diffraction order spot (purely transmitted light). Diffraction is natural for such a gradient metasurface design due to the periodicity of the supercell. The relative intensities of the three main diffraction orders (0, -1 , $+1$) measured at different wavelengths and normalized to the incident intensity are shown in Fig. 4b. The higher diffraction orders are significantly weaker and can be neglected. When the wavelength of the incident beam approaches the optimized position of 705–715 nm, the 0^{th} and all other diffraction orders except -1 are strongly suppressed. The -1 order is, by contrast, enhanced, which corresponds to the transmitted beam deflection to an angle of approximately 10° , in accordance with the theoretical prediction. This is a hallmark of phase-manipulation behavior by a metasurface [6]. For larger wavelengths away from the optimized value the effect disappears and a regular diffraction pattern with strong 0^{th} -order beam spot is again observed (see 775 nm in Fig. 4c).

From Fig. 4b, one can observe that the efficiency of the metasurface reaches the maximum value of around 45% at 705 nm, i.e. 45% of incident light is transformed into the desired (-1) order. The measured values are in very good agreement with numerical calculations for the same design (Figs. S3 and S4 in Supplementary Information). The obtained efficiency is very high in the context of transmissive metasurfaces. It was recently established that for planar

nonmagnetic plasmonic metasurfaces in the lossless case the maximum transmission efficiency is limited to 25% in the crosspolarized beam [40]. This limit appears since the full phase control requires the plasmonic structures to be anisotropic and support more than a single resonance. In order to surpass this limit, the authors of [40] proposed to employ stacked structure of 3 planar metasurfaces. This structure operating at mid-IR frequencies was theoretically shown to have transmission efficiencies around 60%. This value is comparable to our experimental result at visible wavelengths.

Another possibility discussed to get high efficiency in transmission is to employ metasurfaces with both electric- and magnetic-induced currents, which can interfere and cancel the reflection. [41] This approach for nonreflecting metasurfaces proposed in plasmonics is fundamentally similar to our case of dielectric metasurfaces where reflection is cancelled due to interference of electric- and magnetic-dipole resonances. The significant difference between plasmonic and dielectric cases is strong losses, which plasmonic structures have at optical frequencies. In [41] the authors demonstrated this concept at GHz frequencies (where metals are loss-free) with 58 stacks of structured surfaces and could achieve efficiency of $\sim 85\%$ in transmission. Later demonstration of the same concept with plasmonic metasurfaces working at near-IR frequencies could achieve around 30% efficiency in theory and 20% in experiments [42]. This efficiency value is more than twice lower than our experimental data in the visible spectral range.

The efficiency value of around 45% and the total transmitted power through the metasurface obtained in our experiments are lower than the maximum transmission with the single-size nanodisk arrays (around 85%). This can be explained by the variable disk size inside the metasurface and interaction between the neighboring disks of different sizes. The efficiency values can further be improved through careful optimization of the metasurface design taking into account interactions between the neighboring cells.

4. Conclusion

In summary, we have introduced and experimentally demonstrated an all-dielectric metasurface consisting of a subdiffraction array of silicon nanodisks with near-unity broadband transmission at visible wavelengths. The high transmission and greatly suppressed (almost zero) reflection are due to almost complete overlap and interference of simultaneously excited electric and magnetic-dipole resonances in the nanodisks. This allows for full 2π control of phase of the incoming light. In addition, we have verified the metasurface performance by designing a gradient structure for beam deflection. A deflection efficiency of around 45% is demonstrated in the experiment. These results are particularly notable due to the deeply subwavelength periodicity of the design, which ensures that all incident light is interacting with the structure. Finally, the relative simplicity of the fabrication, which utilizes single-layer lithography and thin-film etching, as well as its compatibility with CMOS process, makes this approach promising for integrating the concept of metasurfaces to real-world applications.

Supporting Information

Additional supporting information may be found in the online version of this article at the publisher's website.

Acknowledgements. Y. F. Yu and A. Y. Zhu contributed equally to this work.

The authors are supported by DSI core funds.

Fabrication and scanning electron microscope imaging studies were carried out at the SnFPC cleanroom facility at DSI (SERC Grant 092 160 0139). The authors are grateful to Vytautas Valuckas (NUS/DSI) for SEM imaging. The authors also thank Leonard Gonzaga, Yeow Teck Toh and Doris Ng (DSI) for assistance in the development of various nanofabrication procedures.

Received: 16 February 2015, **Revised:** 18 April 2015,

Accepted: 1 June 2015

Published online: 26 June 2015

Key words: metasurface, silicon nanoparticles, electric-dipole resonance, magnetic-dipole resonance, Kerker's condition.

References

- [1] N. I. Zheludev, *Science* **328**, 582–583 (2010).
- [2] C. L. Holloway, E. F. Kuester, J. A. Gordon, J. O'Hara, J. Booth, and D. R. Smith, *IEEE Antennas Propagat. Mag.* **54**, 10–35 (2012).
- [3] A. V. Kildishev, A. Boltasseva, and V. M. Shalaev, *Science* **339**, 6125 (2013).
- [4] N. Yu and F. Capasso, *Nature Mater.* **13**, 139–150 (2014).
- [5] X. Ni, N. K. Emani, A. V. Kildishev, A. Boltasseva, and V. M. Shalaev, *Science* **335**, 427 (2012).
- [6] N. Yu, P. Genevet, M. A. Kats, F. Aieta, J.-P. Tetienne, F. Capasso, and Z. Gaburro, *Science* **334**, 333–337 (2011).
- [7] S. Sun, K.-Y. Yang, C.-M. Wang, T.-K. Juan, W.T. Chen, C. Y. Liao, Q. He, S. Xiao, W.-T. Kung, G.-Y. Guo, L. Zhou, and D. P. Tsai, *Nano Lett.* **12**, 6223–6229 (2012).
- [8] D. Lin, P. Fan, E. Hasman, and M. L. Brongersma, *Science* **345**, 298–302 (2014).
- [9] P. R. West, J. L. Stewart, A. V. Kildishev, V. M. Shalaev, V. V. Shkunov, F. Strohendl, Y. A. Zakharenkov, R. K. Dodds, and R. Byren, *Opt. Exp.* **22**, 26212–26221 (2014).
- [10] A. Arbabi, Y. Horie, A. J. Ball, M. Bagheri, and A. Faraon, *Nat. Commun.* **6**, 7069 (2015).
- [11] F. Aieta, P. Genevet, M. A. Kats, N. Yu, R. Blanchard, Z. Gaburro, and F. Capasso, *Nano Lett.* **12**, 4932–4936 (2012).
- [12] P. Genevet, N. Yu, F. Aieta, J. Lin, M. A. Kats, R. Blanchard, M. O. Scully, Z. Gaburro, and F. Capasso, *Appl. Phys. Lett.* **100**, 013101 (2012).
- [13] J. Lin, P. Genevet, M. A. Kats, N. Antoniou, and F. Capasso, *Nano Lett.* **13**, 4269–4274 (2013).
- [14] X. Ni, A. V. Kildishev, and V.M. Shalaev, *Nature Commun.* **4**, 2807 (2013).
- [15] U. Levy, C.-H. Tsai, H.-C. Kim, and Y. Fainman, *Opt. Exp.* **12**, 5345–5355 (2004).
- [16] L. Huang, X. Chen, B. Bai, Q. Tan, G. Jin, T. Zentgraf, and S. Zhang, *Light Sci. Appl.* **2**, e70 (2013).
- [17] P. R. West, S. Ishii, G. V. Naik, N. K. Emani, V. M. Shalaev, and A. Boltasseva, *Laser Photon. Rev.* **4**, 795–808 (2010).
- [18] A. Boltasseva and H. A. Atwater, *Science* **331**, 290–291 (2011).
- [19] A. B. Evlyukhin, C. Reinhardt, A. Seidel, B. Luk'yanchuk, and B. N. Chichkov, *Phys. Rev. B* **82**, 045404 (2010).
- [20] A. García-Etxarri, R. Gómez-Medina, L. S. Froufe-Pérez, C. López, L. Chantada, F. Scheffold, J. Aizpurua, M. Nieto-Vesperinas, and J. J. Sáenz, *Opt. Exp.* **19**, 4815–4826 (2011).
- [21] A. Arbabi, Y. Horie, M. Bagheri, and A. Faraon, *arXiv:1411.1494* (2014).
- [22] E. Hasman, V. Kleiner, G. Biener, and A. Niv, *Appl. Phys. Lett.* **82**, 328–330 (2003).
- [23] I. Staude, A. E. Miroshnichenko, M. Decker, N. T. Fofang, S. Liu, E. Gonzales, J. Dominguez, T. S. Luk, D. N. Neshev, I. Brener, and Y. S. Kivshar, *ACS Nano* **7**, 7824–7832 (2013).
- [24] M. Decker, I. Staude, M. Falkner, J. Dominguez, D. N. Neshev, I. Brener, T. Pertsch, and Y. S. Kivshar, *Adv. Opt. Mater.* doi: 10.1002/adom.201400584 (2015).
- [25] J. Cheng, D. Ansari-Oghol-Beig, and H. Mosallaei, *Opt. Lett.* **39**, 6285–6288 (2014).
- [26] P. Lalanne, S. Astilean, P. Chavel, E. Cambril, and H. Launois, *Opt. Lett.* **23**, 1081–1083 (1998).
- [27] Y. Yang, W. Wang, P. Moitra, I. I. Kravchenko, D. P. Briggs, and J. Valentine, *Nano Lett.* **14**, 1394–1399 (2014).
- [28] B.-I. Popa and S. A. Cummer, *Phys. Rev. Lett.* **100**, 207401 (2008).
- [29] Q. Zhao, J. Zhou, F. Zhang, and D. Lippens, *Mater. Today* **12**, 60–69 (2009).
- [30] A. I. Kuznetsov, A. E. Miroshnichenko, Y. H. Fu, J. B. Zhang, and B. Luk'yanchuk, *Sci. Rep.* **2**, 492 (2012).
- [31] A. B. Evlyukhin, S. M. Novikov, U. Zywiets, R. L. Eriksen, C. Reinhardt, S. I. Bozhevolnyi, and B. N. Chichkov, *Nano Lett.* **12**, 3749–3755 (2012).
- [32] L. Shi, T. U. Tuzer, R. Fenollosa, and F. Meseguer, *Adv. Mater.* **24**, 5934–5938 (2012).

- [33] M. Nieto-Vesperinas, R. Gómez-Medina, and J. J. Sáenz, *J. Opt. Soc. Am. A* **28**, 54–60 (2011).
- [34] Y. H. Fu, A. I. Kuznetsov, A. E. Miroshnichenko, Y. F. Yu, and B. Luk'yanchuk, *Nature Commun.* **4**, 1527 (2013).
- [35] S. Person, M. Jain, Z. Lapin, J. J. Sáenz, G. Wicks, and L. Novotny, *Nano Lett.* **13**, 1806–1809 (2013).
- [36] M. Kerker, D.-S. Wang, and C. L. Giles, *J. Opt. Soc. Am.* **73**, 765–767 (1983).
- [37] B. Luk'yanchuk, N. V. Voshchinnikov, R. Paniagua-Dominguez, and A. I. Kuznetsov, *ACS Photon.* doi: 10.1021/acsp Photonics.5b00261 (2015).
- [38] E. E. Radescu and G. Vaman, *Phys. Rev. E* **65**, 046609 (2002).
- [39] A. E. Miroshnichenko, A. B. Evlyukhin, Y. F. Yu, R. M. Bakker, A. Chipouline, A. I. Kuznetsov, B. Luk'yanchuk, B. N. Chichkov, and Y. S. Kivshar, arXiv:1412.0299 (2014).
- [40] F. Monticone, N. M. Estakhri, and A. Alu, *Phys. Rev. Lett.* **110**, 203903 (2013).
- [41] C. Pfeiffer and A. Grbic, *Phys. Rev. Lett.* **110**, 197401 (2013).
- [42] C. Pfeiffer, N. K. Emani, A. M. Shaltout, A. Boltasseva, V. M. Shalaev, and A. Grbic, *Nano Lett.* **14**, 2491–2497 (2014).